Vol. 29 (1998) *ACTA PHYSICA POLONICA B* No 10

RECENT HIGHLIGHTS FROM HERA COLLIDER EXPERIMENTS*

GÜNTER WOLF

DESY — DeutschesElektronen-Synchrotron
Notkestr.85, D-22607 Hamburg, Germany

(Received July 30, 1998)

High statistics data have been presented by ZEUS for hard photoproduction of D^* mesons. The measured cross sections for large $p_\perp^{D^*}$, η^{D^*} lie above those predicted by QCD-NLO calculations. There is a substantial contribution from resolved photons indicating the existence of charm excitation in the photon. Photoproduction of beauty quarks has been observed for the first time by H1. The measured cross section lies above the theoretical expectations calculated in QCD-LO by a substantial factor. First results on quasielastic photoproduction of Upsilons have been presented by ZEUS. The observed cross section lies above the theoretical predictions. QCD-NLO fits to data for the proton structure function F_2 from H1 and ZEUS have provided rather precise determinations of the density of gluons in the proton. The resulting predictions for the charm contribution F_2^c to F_2 are consistent with F_2^c obtained directly from charm production by DIS. An analysis of F_2 data at small Q^2 indicates that the transition from soft hadron-like scattering to DIS occurs somewhere between 0.5 and 3 GeV^2. A QCD-NLO analysis by ZEUS with F_2 measurements starting at $Q^2 = 1$ GeV^2 shows that a good description of the data can be obtained. Surprisingly, while at $Q^2 = 7, 20$ GeV^2 the gluon density (g)at small x is much larger than that for the singlet quarks (Σ), the situation appears to be reversed at $Q^2 = 1$ GeV^2 where $g < \Sigma$. Diffraction dissociation of the virtual photon into high mass hadrons represents a substantial part of the DIS cross section. Its energy dependence is similar to that of the sum of all DIS channels and leads to a pomeron trajectory which lies above that observed in hadron-hadron scattering. The behaviour of the diffractive structure function suggests a substantial contribution from partonic interactions. H1 and ZEUS previously had reported an excess of events above the Standard Model predictions at large Q^2, high x seen in the 1994-96 data. Analysis of the 1997 data, corresponding to about the same integrated luminosity, has not added to this excess.

PACS numbers: 13.60.–r

* Presented at the DESY Zeuthen Workshop on Elementary Particle Theory "Loops and Legs in Gauge Theories", Rheinsberg, Germany, April 19-24, 1998.

1. Introduction

Since the beginning of operation in 1992 the luminosity provided by HERA for H1 and ZEUS has increased by about a factor of two every year thanks to a vigorous machine development program. The increase in luminosity has led to much improved precision *e.g.* in the determination of structure functions and the neutral and charged current cross sections, and has given access to new processes such as the production of heavy quarks. Above all, the two experiments have reached sensitivities for some processes beyond the Standard Model which exceed those of other experiments.

This report presents a snapshot of recent experimental results from H1 and ZEUS for a few selected topics drawing heavily on reports from [1–3]. A recent overview on HERA physics may be found in [4].

Most of the data were obtained with 27.5 GeV positrons colliding with 820 GeV protons equivalent to a total c.m. energy of $\sqrt{s} = 300$ GeV. The useful data correspond to luminosities integrated over 1992-97 of 37 pb^{-1} with e^+p and 1 pb^{-1} with e^-p collisions for H1, and 47 pb^{-1} with e^+p and 1 pb^{-1} with e^-p for ZEUS.

2. Heavy quark production

2.1. Hard $D^{*\pm}$ photoproduction

In photoprodcution processes at HERA, a quasi-real photon ($Q^2 \simeq 0$) is emitted by the incoming lepton and interacts with the proton. At leading order QCD, direct and resolved photon processes can contribute to charm (c) production. The direct process corresponds to photon-gluon fusion, $\gamma g \to c\overline{c}$, while charm quarks in the parton distributions of the photon and the proton can lead to processes of the type $cg \to cg$ known as flavour excitation.

The light quark structure of the photon has been extensively studied in photon-photon collisions at e^+e^- storage rings [5], whilst there is little information at present on the charm content of the photon. Photoproduction of charm with hard transverse momenta is expected to be sensitive to charm excitation.

ZEUS studied photoproduction of $D^{*\pm}$ mesons in dijet events using data from 1996-97 corresponding to an integrated luminosity of 37 pb^{-1} [6]. Events were selected with photon-proton *c.m.* energies of $130 < W < 280$ GeV. The D^* mesons were identified via two decay channels, $D^{*+} \to D^0\pi_S^+ \to (K^-\pi^+)\pi_S^+$ and $D^{*+} \to D^0\pi_S^+ \to (K^-\pi^+\pi^+\pi^-)\pi_S^+$ (plus c.c.). For the analysis of charm with associated dijets, events containing a D^* meson with $p_\perp^{k\pi\pi_S} > 2(4)$ GeV were used. The events were also required to have at least two jets with pseudorapidities $|\eta^{\rm jet}| < 2.4$ and energies $E_T^{\rm jet} > 5$ GeV.

Here η is defined as $-\ln(\tan(\theta/2))$ where the polar angle is measured w.r.t. the direction of the incoming proton. The measured D^* was found to belong to one of the two jets. The differential cross section $d\sigma/dp_\perp^{D^*}$ as obtained from the two D^* decay channels is shown in Fig. 1 for $|\eta^{D^*}| < 1.5$ as a function of $p_\perp^{D^*}$ and in Fig. 2 as a function of η^{D^*} for different minimum values of $p_\perp^{D^*}$. Good agreement between the results from the two D^* channels is observed.

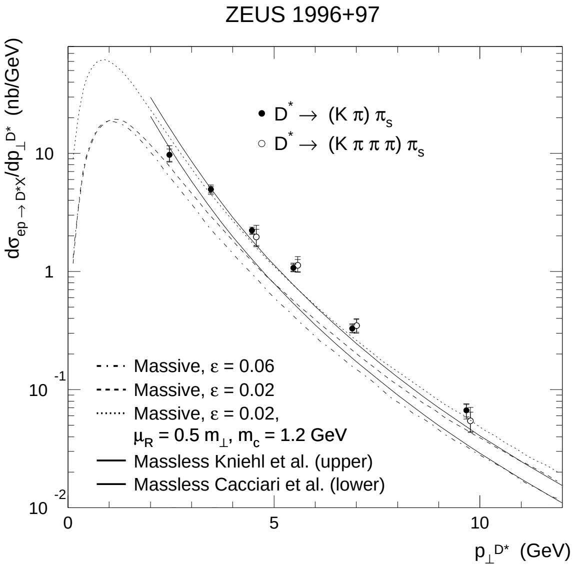

Fig. 1. The differential cross section $d\sigma/dp_\perp$ for D^* photoproduction in the region $130 < W < 280$ GeV, $|\eta^{D^*}| < 1.5$. The curves show the NLO predictions for the massive charm approach (dash-dotted, dashed and dotted) and for the massless approach (full).

The cross sections were compared with NLO QCD calculations in the massive [7] and massless charm schemes using the parton densities CTEQ4M [8] for the proton and GRV-G HO [9] for the photon. The renormalization scale used was $\mu_R = m_\perp = \sqrt{m_c^2 + p_\perp^2}$ ($m_c = 1.5$ GeV) and the factorization scales of the photon and proton structure functions were set to $\mu_F = 2m_\perp$. The charm fragmentaion into D^* was performed using the Peterson function [10] $f(z) \propto [z(1 - 1/z - \epsilon/(1-z))^2]^{-1}$. Here z is the fraction of the quark momentum carried by the D^* and ϵ is a free parameter. Data from e^+e^- suggest a value of $\epsilon = 0.02$ while [7] used $\epsilon = 0.06$. The cross sections predicted by the massive scheme shown in Figs. 1 and 2 are considerably lower than those measured. The shapes predicted for the η distributions are also inconsistent with the data.

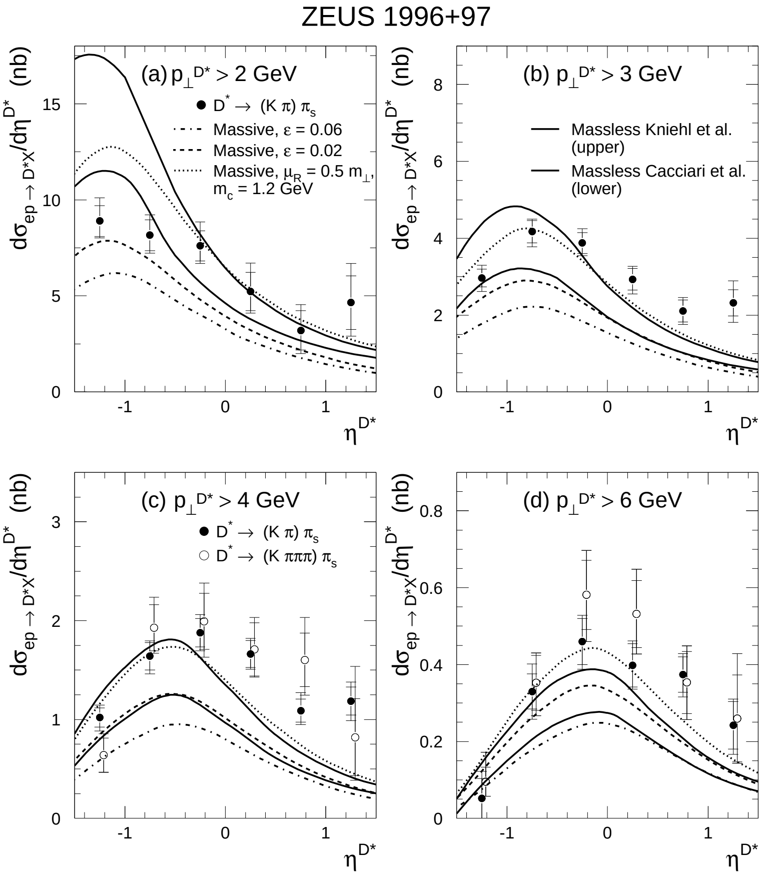

Fig. 2. The differential cross section $d\sigma/d\eta^{D^*}$ for D^* photoproduction in the region $130 < W < 280$ GeV for different minimum values of $p_\perp^{D*}$. The curves show the NLO predictions for the massive charm approach (dash-dotted, dashed and dotted) and for the massless approach (full).

The massless charm scheme assumes the charm to be an active flavour in both the proton and the photon [11–13]. Results from two different massless calculations are shown in Figs. 1 and 2. They agree in shape with each other but disagree in magnitude. The predicted cross sections are in general below the data, most notably in the forward direction ($\eta^{D^*} > 0$).

In summary, the measured cross sections for D^* photoproduction for $p_\perp^{D^*} > 4$ GeV, $\eta^{D^*} > 0.5$ lie above the current QCD NLO predictions by a factor of about 1.4 - 2.

Using the tranverse energies and angles of the jets, separation into D^* events produced predominantly by direct photons and those produced by resolved photons was performed. The presence of a substantial contribution from resolved photon processes indicates the existence of charm excitation in the photon.

2.2. Hard beauty photoproduction

In a pioneering analysis H1 has presented a first measurement of beauty (b) production at HERA [14]. The b-quarks were identified via their semileptonic decay $b \to \mu\nu X$.

The analysis was performed with data from 1995-96 corresponding to an integrated luminosity of 8.3 pb^{-1}. Events were selected requiring at least two jets, each with transverse energy $E_T > 6$ GeV plus at least one muon in the central detector with $p_T^\mu > 2$ GeV being associated with one of the jets. The contribution from b-quarks was separated from those of charm and light-quark background on a statistical basis using the muon transverse momentum relative to the thrust axis of the jet, $p^\mu_{T,\mathrm{rel}}$.

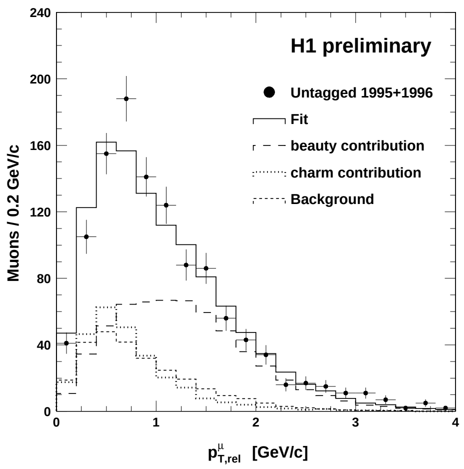

Fig. 3. The measured $p^\mu_{T,\mathrm{rel}}$ distribution (points with error bars) and the result of the fit for the different components (histograms). From H1 [14].

The distribution of $p^\mu_{T,\mathrm{rel}}$ is shown in Fig. 3. The bulk of the events have small $p^\mu_{T,\mathrm{rel}} < 1$ GeV stemming from misidentified hadrons, from muons from π, K decays and from charm decay. In addition, there is a substantial number of events with $p^\mu_{T,\mathrm{rel}} > 1.5$ GeV. The shape of the first two contributions were estimated from an analysis of identified π's. The expected shapes of the charm and beauty contributions were calculated in LO using the AROMA model [15]. From a fit to the measured $p^\mu_{T,\mathrm{rel}}$ spectrum the size of these contributions were determined. They are shown by the histograms in Fig. 3. The prediction for the sum of all contributions describes the data well. For $p^\mu_{T,\mathrm{rel}} > 2$ GeV the events arise predominantly from b-decay.

The distribution of the pseudorapidity $\eta^{\rm jet}$ of the jet containing the muon is shown in Fig. 4. Most of the events have $\eta^{\rm jet}$ values between -0.5 and $+1.0$. The measured distribution is well reproduced by the prediction (histogram).

The cross section for b-production in the kinematic region $0.1 < y_{JB} < 0.8$, where $W^2 \approx y_{JB}s$, $p_T^{\mu} > 2$ GeV, $35^o < \theta^{\mu} < 130^o$ was found to be

$$\sigma_{\rm vis}(ep \to b\bar{b}X) = 0.93 \pm 0.08({\rm stat})^{+0.21}_{-0.12}({\rm syst}){\rm nb}. \tag{1}$$

Taken at face value the observed b-production is a factor of ≈ 5 higher than the value of 0.19 nb predicted by AROMA in LO. The HERWIG model [16] yielded a value similar to that of AROMA. This excess of data over theory is similar to the results found for $b\bar{b}$ production in $p\bar{p}$ collisions.

As a next step, a comparison with NLO calculations of photoproduction of b-quarks is needed. Also, an analysis which studies in a general manner to what extent the available charm and beauty data constrain the gluon and heavy quark densities of the photon, is highly desirable.

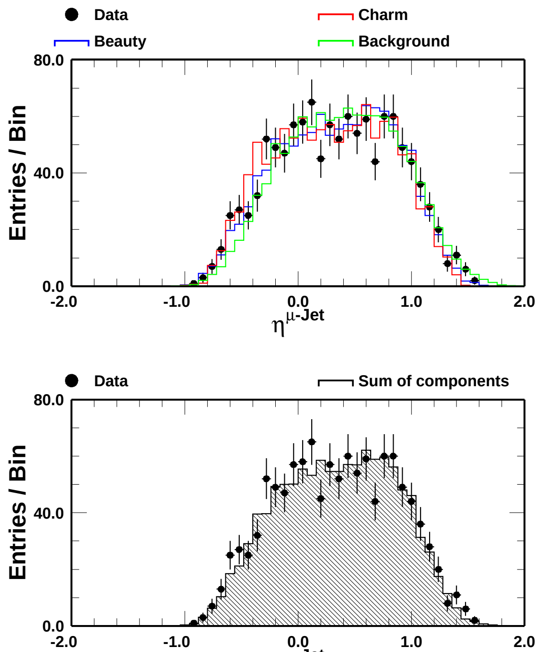

Fig. 4. The pseudorapidity distribution of the jet containing the muon for the data (points with error bars) and the result of the fit for the different components (histograms). From H1 [14].

2.3. Quasielastic photoproduction of charmonium and bottonium

The cross section for quasi-elastic photoproduction of light onia such as $\gamma p \to Vp$ with $V = \rho^0, \phi$ is rather constant as a function of the total c.m. energy W, $\sigma_{\gamma p \to Vp} \propto W^\delta$ with $\delta \approx 0.2$. This behaviour is similar to that of elastic hadron-hadron scattering and is expected in a combined Vector Dominance Model Regge approach. In contrast, $\sigma_{\gamma p \to J/\Psi p}$ rises rapidly with W as shown by Fig. 5. Here $\delta \approx 0.9$, see Fig. 5(a). Such a behaviour is expected in pQCD in which the reaction proceeds by two-gluon exchange between the photon and the incoming proton [18]. The pQCD models describe both the W dependence and magnitude of $\sigma_{\gamma p \to J/\Psi p}$ as shown by the curves in Fig. 5(b). The importance of pQCD contributions in $\gamma p \to J/\Psi p$ can be understood as a consequence of the heavy mass of the charm quark mass which sets a hard scale.

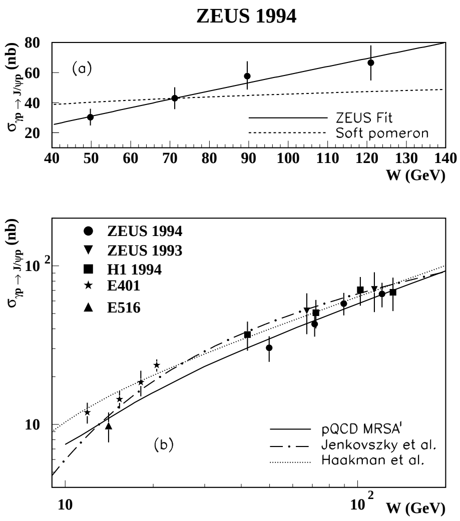

Fig. 5. The cross section for $\gamma p \to J/\Psi p$ as a function of the c.m. energy W. (a) Shows a fit of the ZEUS data to the expression $\sigma_{\gamma p \to J/\Psi p} \propto W^\delta$. The dashed line shows the predictio of a soft pomeron model in which $\delta \approx 0.22$. (b) The data from H1, ZEUS and lower energy measurements are compared with pQCD predictions by [18] (solid line), [19] (dotted line) and [20] (long dash dotted line). From [17].

Recently, ZEUS reported first evidence for the quasielastic photoproduction of the Upsilon [21]. The Upsilon was observed in the 1995-97 data corresponding to an integrated luminosity of 43 pb^{-1}. Figure 6 shows the $\mu^+\mu^-$ mass spectrum for events where besides the two muons no other particles were observed in the central detector. Strong J/Ψ and Ψ' signals are observed on top of a large background coming from the Bethe-Heitler process. In addition, there is a signal for Υ production. The limited statistics

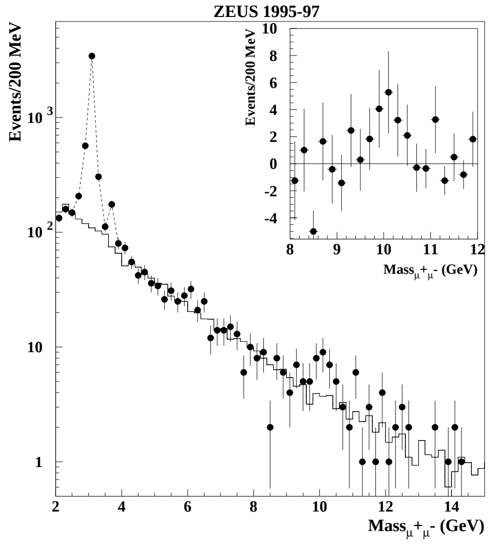

Fig. 6. Mass distribution of $\mu^+\mu^-$ pairs from photoproduction. The histogram represents the simulated Bethe-Heitler background. Points in the J/Ψ region are connected by a dotted line. The insert shows the signal remaining in the Υ region after subtraction of the non-resonant background. From ZEUS [21].

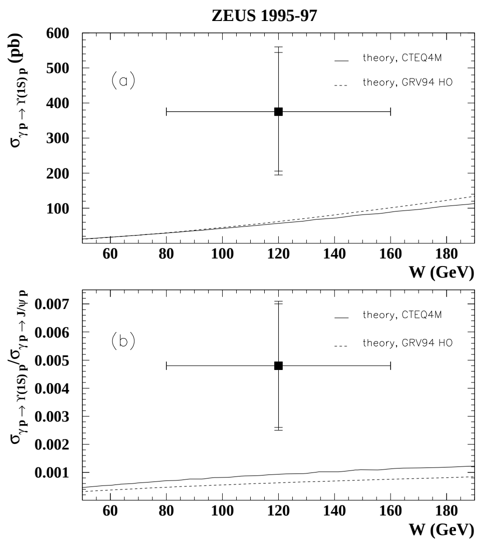

Fig. 7. (a) $\sigma_{\gamma p\to\Upsilon(1S)p}$ and (b) the ratio $\sigma_{\gamma p\to\Upsilon(1S)p}/\sigma_{\gamma p\to J/\Psi p}$ as a function of W. Data (points with error bars) are compared with the predictions of [22] for different parton densities of the proton (dashed and full lines).

does not allow to distinguish between the $\Upsilon(1S), \Upsilon(2S), \Upsilon(3S)$ states. Assuming that the cross sections times branching ratios for the three states are the same as measured in $p\overline{p}$ interactions gave for the cross section

$$\sigma_{\gamma p \to \Upsilon(1S)p} = 375 \pm 170(\mathrm{stat})^{+75}_{-64}(\mathrm{syst})\mathrm{pb} \ \text{ at } W = 120 \text{ GeV} \tag{2}$$

and for the ratio

$$\sigma_{\gamma p \to \Upsilon(1S)p}/\sigma_{\gamma p \to J/\Psi p} = (4.8 \pm 2.2(\mathrm{stat})^{+0.7}_{-0.6}(\mathrm{syst})) \times 10^{-3}. \tag{3}$$

In Fig. 7 these values are compared with theoretical calculations [22] which predict $\sigma_{\gamma p \to \Upsilon(1S)p} \approx 60$ pb and $\sigma_{\gamma p \to \Upsilon(1S)p}/\sigma_{\gamma p \to J/\Psi p} \approx 10^{-3}$, both weakly dependent on the structure function parametrisation used. At face value, the data exceed the predictions by a factor of about 5. It remains to be seen whether this discrepancy persists with more precise data.

3. Structure functions of the proton

Measurements of deep inelastic neutral current scattering by H1 and ZEUS have shown a rapid rise of the structure function $F_2(x, Q^2)$ as $x \to 0$. In QCD, this rise is attributed to a rapid rise of the quark momentum densities $xq(x, Q^2)$ in the proton, $F_2(x, Q^2) = \sum_q e_q^2 xq(x, Q^2)$ (e_q is the electric charge of quark type q).

The gluon density $g(x, Q^2)$ of the proton at small x and large Q^2 dominates the scale breaking of $F_2(x, Q^2)$,

$$\frac{dF_2}{d\ln Q^2} = \sum_q e_q^2 \frac{\alpha_s(Q^2)}{2\pi} \int_x^1 \frac{dy}{y}[P_{qq}(\frac{x}{y})q(y, Q^2) + P_{qg}(\frac{x}{y})g(x, Q^2)]. \tag{4}$$

Here, P_{qq} and P_{qg} are the quark and gluon splitting functions. The gluon density has been extracted from the F_2 data primarily by DGLAP type QCD fits and has also been found to rise rapidly as $x \to 0$.

Until recently, most of the information had come from data taken until 1994 and corresponding to about 2–3 pb^{-1} per experiment. Now, analyses have become available which are based on much larger statistics by including data from 1995-96 running. Furthermore, the region covered in x, Q^2 has been enlarged substantially; in particular, ZEUS, and also H1, have started to map out the transition region from photoproduction to deep inelastic scattering in the region of $x = 10^{-4}$–10^{-6}. Progress has also been made in the measurement of the charm contribution to F_2 which provides for a direct test of $g(x, Q^2)$ extracted with a QCD fit from the F_2 data.

3.1. Structure function F_2 in the DIS regime

Figure 8 shows preliminary results for F_2 as a function of x from H1 [23] for $2 < Q^2 < 90$ GeV^2 obtained from 1995-96 running which present a substantial improvement over the 1994 data. The curves show the results of a QCD NLO fit which describe the data well. In Fig. 9 the data are displayed for fixed x as a function of Q^2. The QCD fit is seen to describe the data well from $Q^2 = 2$ GeV^2 up to 5000 GeV^2.

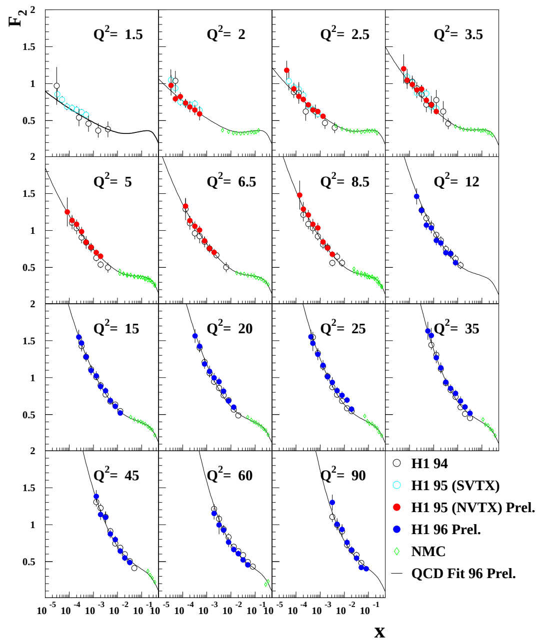

Fig. 8. Preliminary data from H1 for the structure function F_2 as a function of x for fixed values of Q^2. Also included are data from NMC. The curves show a QCD NLO fit to the data.

The gluon momentum density $xg(x, Q^2)$ of the proton as determined from the QCD NLO fits by H1 and ZEUS at $Q^2 = 20$ GeV^2 is shown in Fig. 10 together with a measurement performed by NMC at large x. The H1 and ZEUS results are found to agree within errors. The precision now achieved for $xg(x, Q^2)$ is around 15% at $x = 5.10^{-4}$. The gluon momentum density is seen to rise fast as $x \to 0$. Other QCD NLO fits (MRSR1, CTEQ4M), which include the HERA data, obtained similar results as shown by the curves in Fig. 10. In the GRV94 model [25] the quark and gluon densities of the proton are assumed to have valence like distributions at $Q_0^2 = 0.34$ GeV^2 chosen as the starting value for the QCD evolution. The GRV94 model predicts a somewhat steeper rise than observed by H1 and ZEUS.

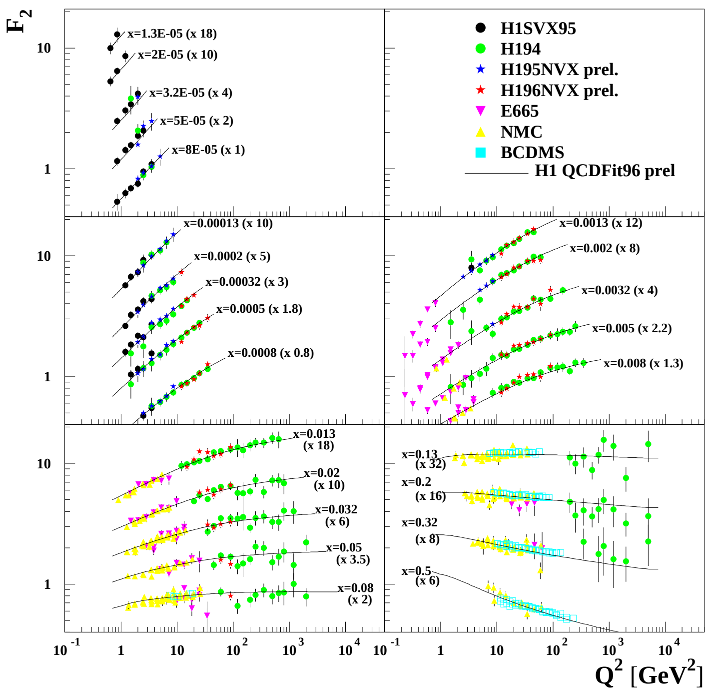

Fig. 9. Preliminary data from H1 for the structure function F_2 as a function of Q^2 for fixed values of x. Also shown are data from NMC, BCDMS and E665. The curves show a QCD NLO fit to the data.

The production of charm quarks in DIS is believed to proceed predominantly via fusion of the virtual photon with a gluon from the proton. The charm contribution to DIS was determined by observing D^* production in a limited $\eta^{D^*}, p_\perp^{D^*}$ region. The measured cross section $\sigma(ep \to eD^*X)$ was extrapolated to the full range in $\eta^{D^*}, p_\perp^{D^*}$ with the help of a QCD model. Using the branching ratio for $c \to D^*$ measured at LEP and the cross section $\sigma(ep \to ec\bar{c}X)$ the charm contribution $F_2^c(x, Q^2)$ is determined [24, 26]. Figure 11 shows F_2^c as a function of x for fixed Q^2 values between 3 and 170 GeV^2. A comparison with the F_2 data shows that for $Q^2 \geq 7$ GeV^2 charm contributes about 20 - 30% of F_2. This is in agreement with the ratio of $4/9$ expected for a democratic sea assuming massless quarks and neglecting the b quark contribution.

The curves in Fig. 11 show the prediction for F_2^c using the gluon density as obtained from the QCD fit to F_2. They are consistent with the data providing an important test for the QCD analyses and fits performed by H1 and ZEUS on F_2. For a recent discussion of the theoretical uncertainties in the determination of F_2^c see [27].

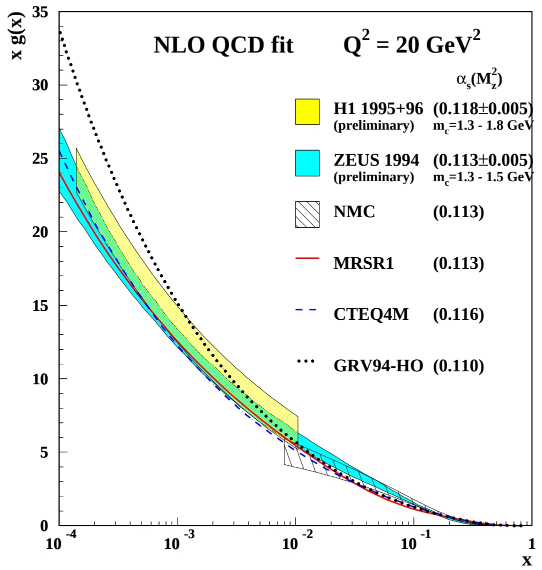

Fig. 10. Preliminary data from H1 and ZEUS for the gluon momentum density of the proton as a function of x at $Q^2 = 20$ GeV^2.

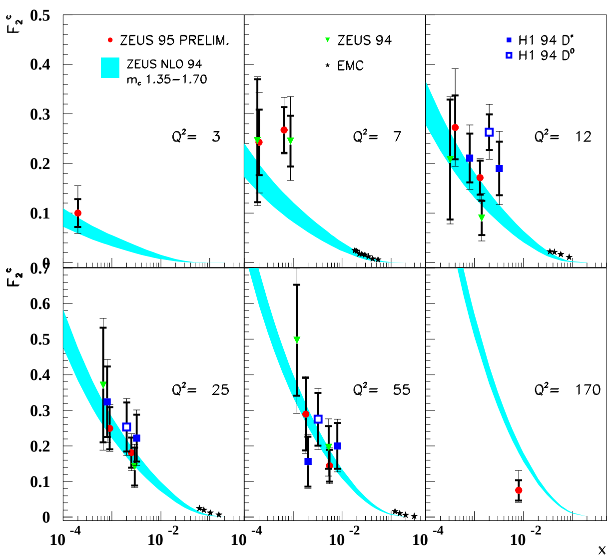

Fig. 11. The charm contribution $F_2^c(x, Q^2)$ to the proton structure function F_2 for fixed Q^2 as a function of x as measured by EMC, H1 and ZEUS. The 1995 data from ZEUS are preliminary. The bands show the predictions (including the uncertainties) obtained from the ZEUS NLO fit to the 1994 F_2 data.

3.2. F_2 in the transition region between photoproduction and DIS

The structure function $F_2(x,Q^2)$ vanishes as $Q^2 \to 0$, as can be seen from its relation with the total virtual photon proton cross section, which is nonzero for $Q^2 = 0$:

$$\sigma^{\rm tot}_{\gamma * p}(W,Q^2) \approx \frac{4\pi^2\alpha}{Q^2} F_2(x = Q^2/W^2, Q^2). \tag{5}$$

Measurements of F_2 at small Q^2 and small $x < 10^{-4}$ were published by H1 [28] and ZEUS [29]. Additional measurements were presented in [30]. Figure 12 shows F_2 for fixed x as a function of Q^2. Comparison with phenomenological models (see [4,29] for further discussions) showed that Vector Dominance type models combined with a Regge approach (*e.g.* DL [31]) can reproduce the Q^2, x behaviour of F_2 up to $Q^2 \approx 0.5$ GeV^2 but fail to reproduce the steep rise at larger Q^2. The QCD based model of GRV, on the other hand, gives a good account of this rise. The comparison suggests that the transition from soft to hard scattering occurs at Q^2 values somewhere between 0.5 and 3 GeV^2.

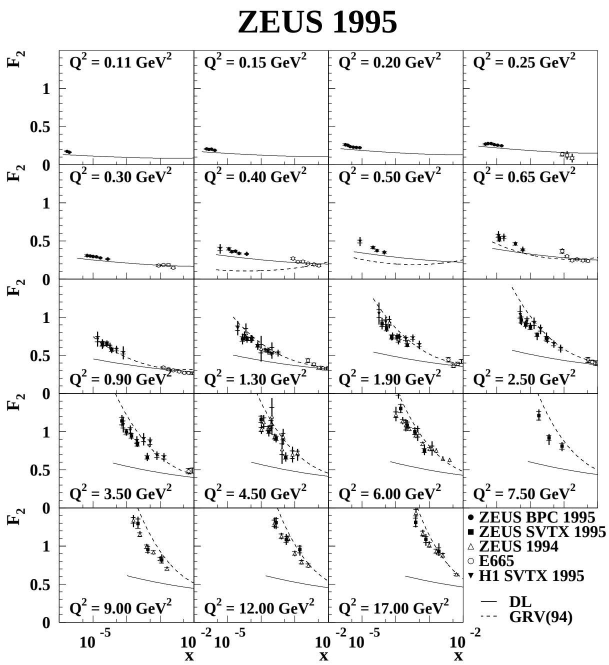

Fig. 12. F_2 as a function of Q^2 for fixed values of x. The curves show predictions of the DL and GRV94 models and of ALLM which is a parametrisation of the HERA data.

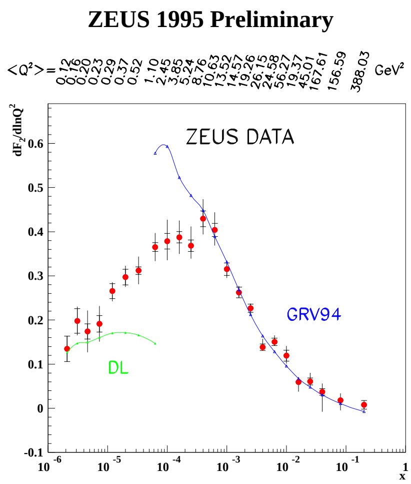

Fig. 13. $dF_2/d\ln Q^2$ as a function of x calculated by fitting ZEUS F_2 data in bins of x to the functional form $a + b\ln Q^2$. For each x bin the average Q^2 value is indicated on top of the figure. The linked points labelled DL and GRV94 are from the Donnachie-Landshoff Regge fit and the GRV94 NLO QCD fit. In both cases, the points are obtained using the same Q^2 range as for the experimental data. From ZEUS.

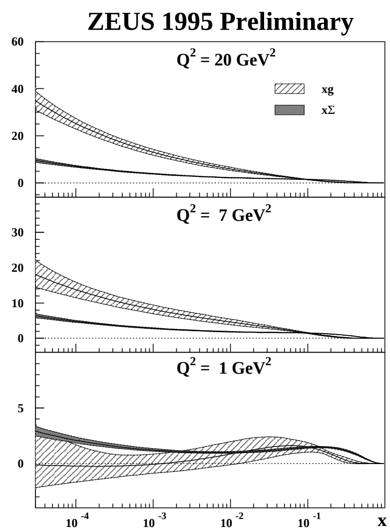

Fig. 14. The quark singlet momentum distribution, $x\Sigma(x,Q^2)$ (shaded), and the gluon momentum density, $xg(x,Q^2)$ (hatched), as a function of x at fixed values of $Q^2 = 1, 7, 20$ GeV^2. The error bands correspond to the quadratic sum of all errors. From ZEUS.

ZEUS studied also the scaling violations, $dF_2/d\ln Q^2$, in the transition region [1,32]. The logarithmic slope $dF_2/d\ln Q^2$ was derived from the data by fitting $F_2 = a + b\ln Q^2$ in bins of fixed x for $W^2 \simeq Q^2/x > 10$ GeV^2. Figure 13 shows $dF_2/d\ln Q^2$ as a function of x (Caldwell plot). Also shown (on top of figure) for each x bin is the weighted mean of Q^2 ($< Q^2 >$) which increases as x increases due to kinematics and detector acceptance. For x values down to 3×10^{-4} the slope $dF_2/d\ln Q^2$ increases as x increases. At lower x (equivalent to lower Q^2) values the slope decreases. The prediction of the GRV94 model, for which $dF_2/d\ln Q^2$ was determined in the same manner as for the data, reproduces the data for $x > 3 \times 10^{-4}$ ($Q^2 > 8$ GeV^2). For smaller x, the GRV94 slope keeps on rising while in the data it decreases.

In order to gain further insight into the scaling violations at low x and Q^2 ZEUS performed QCD NLO fits using all their data with $3\times10^{-5} < x < 0.7$ and $Q^2 > 1$ GeV^2 together with those from NMC [33] and BCDMS [34]. A reasonable description of the data was achieved by the fits. Figure 14 shows the singlet quark momentum density ($x\Sigma \equiv x\sum_q[q(x) + \overline{q}(x)]$) and the momentum density of the gluon as a function of x for $Q^2 = 1,\ 7$ and 20 GeV^2. For $Q^2 \geq 7$ GeV^2 the gluon density is much larger than the singlet quark density while at $Q^2 = 1$ GeV^2 the gluon density has become equal or lies below the singlet quark density. Also, $x\Sigma$ is seen to rise as $x \to 0$ for all three Q^2 values; xg , on the other hand, rises at $Q^2 = 7$ and 20 GeV^2 but may be flat at $Q^2 = 1$ GeV^2. Such a behaviour was also found by [35].

One may tentatively conclude that at low Q^2, of the order of 1 GeV^2, the quark sea drives the gluon density while at higher Q^2 the gluon drives the density of the sea quarks. However, this conclusion may be premature since the fits did not allow for a contribution from soft scattering which could still be substantial at $Q^2 \geq 1$ GeV^2 (see *e.g.* Fig. 12).

4. Diffraction in DIS

Diffraction has been studied extensively in hadron-hadron scattering at small momentum transfers [36]. An elegant parametrization of the data has been provided by the Regge formalism through the introduction of a pomeron trajectory [37]. The hypothesis that diffraction may have a partonic component [39] has been substantiated by the observation of high transverse energy jets produced in $p\overline{p}$ scattering [40]. However, in hadron-hadron scattering both collision partners are extended objects which makes extraction of the underlying partonic process(es) difficult. In DIS, on the other hand, the virtual photon has a pointlike coupling to quarks. HERA offers a unique opportunity to study the partonic structure of diffraction since it gives access to the regime of large photon virtualities and large energy transfers between the virtual photon and the target proton in its rest system, $\nu = Q^2/(2m_p x) = 2 - 20$ TeV.

Diffraction in virtual photon proton scattering has been studied at HERA in the quasielastic processes $\gamma^* p \to Vp$, where $V = \rho^0, \omega, \phi, J/\Psi, \Upsilon$. While low mass V production ($V = \rho^0, \omega, \phi$) contributes more than 10% of the total cross section at $Q^2 = 0$ [41] it becomes negligible at large Q^2 [42]. However, diffractive dissociation of the virtual photon, $\gamma^* p \to XN$ (N= proton or a low mass nucleon system), into a large mass M_X, first recognized by the presence of a class of events with a large rapidity gap [43, 44] remains a substantial fraction of the total DIS cross section also at large Q^2 [45]. This has opened a window for a systematic study of diffraction in reactions initiated by a hard probe [45–51].

4.1. t-dependence of the diffractive cross section

The dependence of the diffractive cross section $d\sigma_{\gamma^* p \to Xp}/dM_X$ on the square of the four-momentum transfer t between the incoming and outgoing proton was measured by ZEUS by detecting the scattered proton in the leading proton spectrometer (LPS) and the system X in the central detector [50]. The cross section is steeply falling with $-t$ as shown in Fig. 15. A fit of the form $d\sigma_{\gamma^* p \to Xp}/dM_X \propto exp(bt)$ yielded $A = 7.2 \pm 1.1(\mathrm{stat})^{+0.7}_{-0.9}(\mathrm{syst})$

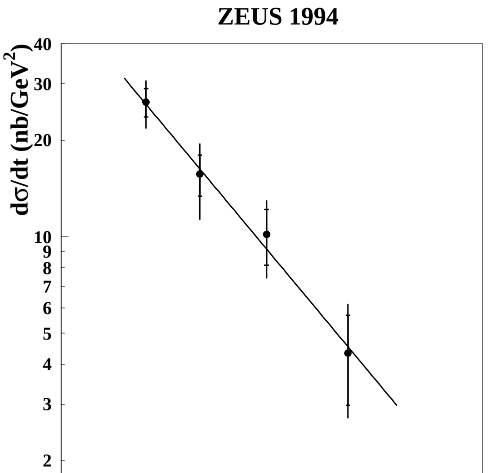

Fig. 15. The diffractive cross section $d\sigma_{\gamma^* p \to Xp}/dM_X$ for events with a leading proton carrying more than 97% of the incoming proton momentum, $5 < Q^2 < 20$ GeV^2, $50 < W < 270$ GeV and $0.015 < \beta \approx Q^2/(M_X^2 + Q^2) < 0.5$. From ZEUS.

GeV^{-2}. This shows that small momentum transfers between incoming and outgoing proton dominate as expected for diffractive scattering.

4.2. Diffractive structure function and cross section

Isolation of diffractive events with the LPS is rather straightforward: detection of a proton scattered under very small angles and carrying a large fraction of the momentum of the incoming proton, $x_L = p^{LPS}/p_{p_{\rm beam}} > 0.95$ ensures a large rapidity gap between the outgoing proton and the system X. However, the event rate is limited by the acceptance of the LPS.

In QCD, diffraction is characterized by the exchange of a colourless object, *e.g.* a colour singlet two-gluon system, between the incoming virtual photon and proton. The exchange of a colourless system suppresses the QCD radiation, and therefore the production of hadrons, in comparison with nondiffractive scattering. Large acceptance for diffractive events has been achieved by requiring either a large rapidity gap between the nucleonic system N produced in the forward direction and the system X detected in the central detector, or by using the fact that in diffractive events most of the hadronic energy is carried away by the system N which escapes detection leaving behind, in the region of the central detector, a low mass system: by measuring the distribution of the mass of the hadronic system observed in the central detector the diffractive contribution can be separated from the nondiffractive one. Analyses based on the first method were performed by H1 [47, 49] and based on the second method by ZEUS [48, 51].

The results were presented in terms of the diffractive cross section $d\sigma_{\gamma^* p\to Xp}/dM_X$ and the diffractive structure function $F_2^{D(3)}(x_{I\!P}, \beta, Q^2)$ [39]. The cross section for the process $ep \to eXN$ can be expressed in terms of the transverse (T) and longitudinal (L) cross sections, $\sigma_T^{\rm diff}$ and $\sigma_L^{\rm diff}$, for $\gamma^* p \to XN$ as:

$$\begin{aligned} \frac{d\sigma^{\rm diff}_{\gamma^* p\to XN}(M_X, W, Q^2)}{dM_X} &\equiv \frac{d(\sigma_T^{\rm diff}+\sigma_L^{\rm diff})}{dM_X} \\ &\approx \frac{2\pi}{\alpha}\,\frac{Q^2}{(1-y)^2+1}\,\frac{d\sigma^{\rm diff}_{ep\to eXN}(M_X, W, Q^2)}{dM_X\, d\ln W^2 dQ^2}\,. \end{aligned} \tag{6}$$

The diffractive structure function of the proton can be related to the diffractive cross section in terms of the scaling variables $x_{I\!P} \approx (M_X^2+Q^2)/(W^2+Q^2)$ and $\beta \approx Q^2/(M_X^2+Q^2)$. In models where diffraction is described by the t-channel exchange of a system, for example the pomeron, $x_{I\!P}$ is the momentum fraction of the proton carried by this system and β is the momentum fraction of the struck quark within this system. One obtains [52]:

$$\frac{1}{2M_X}\frac{d\sigma^{\rm diff}_{\gamma^*p\to XN}(M_X,W,Q^2)}{dM_X} = 4\pi^2\alpha\frac{W^2}{(Q^2+W^2)^2Q^2}F_2^{D(3)}(\beta,x_{I\!P},Q^2). \quad (7)$$

For $W^2 \gg Q^2$, Eq. (7) can be written as:

$$\frac{1}{2M_X}\frac{d\sigma^{\rm diff}_{\gamma^*p\to XN}(M_X,W,Q^2)}{dM_X} \approx \frac{4\pi^2\alpha}{Q^2(Q^2+M_X^2)}x_{I\!P}F_2^{D(3)}(\beta,x_{I\!P},Q^2). \quad (8)$$

If $F_2^{D(3)}$ is interpreted in terms of quark densities then it specifies for a diffractive process the probability to find a quark carrying a momentum fraction $x = \beta x_{I\!P}$ of the proton momentum.

4.3. Diffractive structure function measurement by H1

H1 presented their results for $\gamma^*p \to XN$ in terms of the diffractive structure function. The mass of the nucleon system N was restricted to $M_N < 1.6$ GeV. In Fig. 16, $x_{I\!P}F_2^{D(3)}$ is shown as a function of $x_{I\!P}$ for fixed β values and fixed Q^2 between 4.5 and 75 GeV^2. The variation of $x_{I\!P}F_2^{D(3)}$ with β and Q^2 is rather modest, indicating moderate scaling violations. In general, $x_{I\!P}F_2^{D(3)}$ is falling in the region $x_{I\!P} \leq 10^{-2}$ followed sometimes by an increase for large $x_{I\!P}$ values. The $x_{I\!P}$ dependence of $F_2^{D(3)}$ is related to the W dependence of the diffractive cross section and, if analyzed in a Regge approach, to the Regge trajectories of the t-channel exchanges. By writing $x_{I\!P}F_2^{D(3)}(x_{I\!P},\beta,Q^2) = (C/x_{I\!P})\cdot(x_0/x_{I\!P})^n F_2^{D(2)}(\beta,Q^2)$, $n = 2(\overline{\alpha_{I\!P}}-1)$ if only the pomeron trajectory $\alpha_{I\!P}$ (here averaged over t) is contributing. Because of the rise of $x_{I\!P}F_2^{D(3)}$ seen at large $x_{I\!P}$, H1 concluded that in addition to the pomeron a lower lying trajectory R is also contributing. The solid curves in Fig. 16 show the result of a two-component fit to the data. The dashed curves show the pomeron contribution alone as obtained from the fit. The fit yielded for the intercept of the pomeron trajectory $\alpha_{I\!P}(0) = 1.203 \pm 0.020(\text{stat}) \pm (0.013(\text{syst})^{+0.030}_{-0.035}(model)$, a value which is above the results deduced from (soft) hadron-hadron scattering where $\alpha_{I\!P}(0) = 1.08$ [38] and $1.096^{+0.012}_{-0.009}$ [53] was found.

A fit was performed to the data using a QCD motivated model, in which parton distributions are assigned to the leading and subleading exchanges. Figure 17 shows the resulting contributions to the parton densities of the pomeron as a function of the fraction z of the pomeron momentum carried by the parton. Within this model the majority of the momentum of the pomeron is found to be carried by gluons.

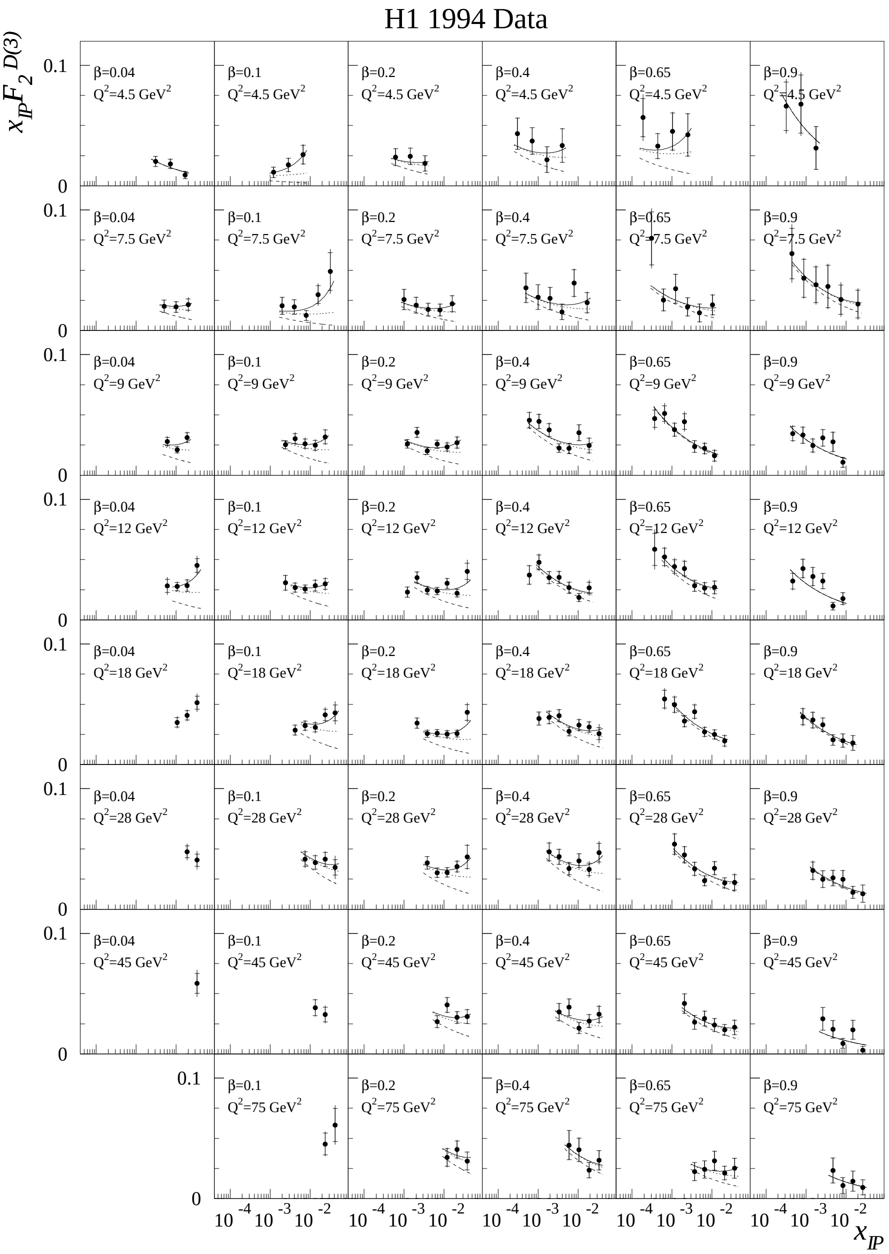

Fig. 16. The differential structure function $x - I\!PF_2^{D(3)}$ as a function of $x_{I\!P}$ for various β and Q^2 values. The solid curves show the results from the two-component Regge fit. The dashed curves show the pomeron contribution alone. From H1.

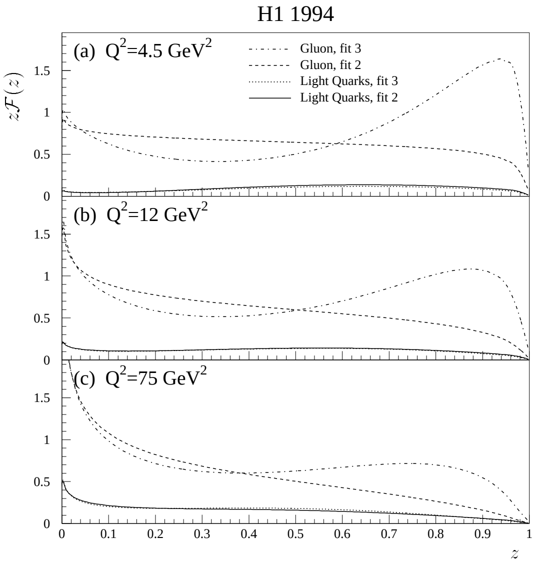

Fig. 17. The sum of the light quark and gluon distributions as a function of the momentum fraction z of the pomeron carried by the parton at different values of Q^2. From H1.

4.4. Diffractive cross section and structure function measured by ZEUS

ZEUS determined the diffractive cross section and structure function for $\gamma^* p \to XN$ where $M_N < 5.5$ GeV. The diffarctive cross section is presented in Fig. 18 as a function of W for various M_X and Q^2 values. The diffractive cross section rises rapidly with W at all Q^2 values for M_X up to 7.5 GeV. A fit to the form

$$\frac{d\sigma^{\rm diff}_{\gamma^* p \to XN}(M_X, W, Q^2)}{dM_X} = h \cdot W^{a^{\rm diff}}\,, \tag{9}$$

where $a^{\rm diff}$ and the normalization constants h were treated as free parameters, yielded $a^{\rm diff} = 0.507 \pm 0.034({\rm stat})^{+0.155}_{-0.046}({\rm syst})$ which corresponds to a t-averaged $\overline{\alpha_{I\!P}} = 1 + a^{\rm diff}/4 = 1.127 \pm 0.009({\rm stat})^{+0.039}_{-0.012}({\rm syst})$. This value is consistent with the H1 result since averaging over the t-distribution gives approximately $\overline{\alpha_{I\!P}} = \alpha_{I\!P}(0) - 0.03$.

The diffractive cross section was compared with the measured total virtual-photon proton cross section. The ratio of the two cross sections,

$$r^{\rm diff}_{\rm tot} = \frac{\int_{\mathbf{M_a}}^{\mathbf{M_b}} dM_X \, d\sigma^{\rm diff}_{\gamma^* p \to XN}/dM_X}{\sigma^{\rm tot}_{\gamma^* p}}, \tag{10}$$

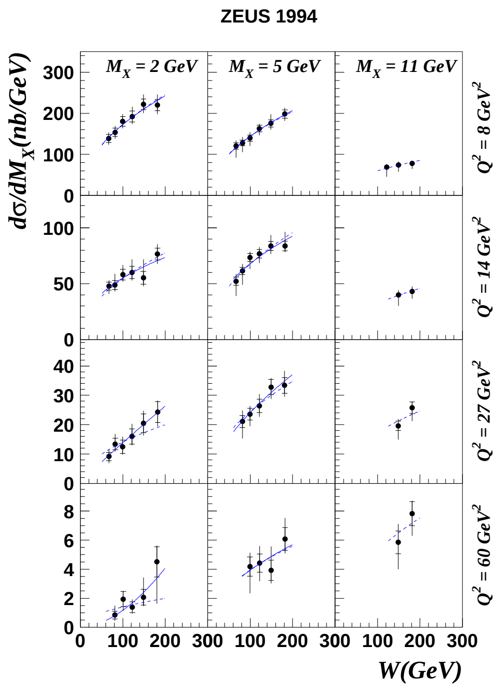

Fig. 18. The diffractive cross section $d\sigma^{\rm diff}_{\gamma^* p\to XN}/dM_X$, $M_N < 5.5$ GeV, as a function of W for different M_X and Q^2 values. The solid curves show the result from fitting the diffractive cross section for each (W, Q^2) bin separately using the form $d\sigma^{\rm diff}_{\gamma^* p\to XN}/dM_X \propto (W^2)^{a^{\rm diff}}$ where $a^{\rm diff}$ and the normalization constants were treated as free parameters. The dashed curves show the result from the fit where $a^{\rm diff}$ was assumed to be the same for all (W, Q^2) bins. From ZEUS.

is displayed in Fig. 19 as a function of W for the different M_X bins and Q^2 values. The data show that, for fixed M_X, contrary to naive expectations, the diffractive cross section possesses the same W dependence as the total cross section. The rapid rise of $\sigma_{\rm tot}$ with W, which is equivalent to the rapid rise of F_2 as $x \to 0$, in QCD is attributed to the evolution of partonic processes. The observation of similar W dependences for the total and diffractive cross sections suggests, therefore, that diffraction in DIS receives sizeable contributions from hard processes. The same W dependence for the diffractive and total cross sections was predicted in [54].

The diffractive structure function, multiplied by $x_{I\!P}$ is shown in Fig. 20 as a function of $x_{I\!P}$ for different values of β and Q^2. $x_{I\!P} F_2^{D(3)}(x_{I\!P}, \beta, Q^2)$ decreases with increasing $x_{I\!P}$, which reflects the rapid increase of the diffractive cross section with rising W. The data are consistent with the assumption that the diffractive structure function $F_2^{D(3)}$ factorizes into a term depend-

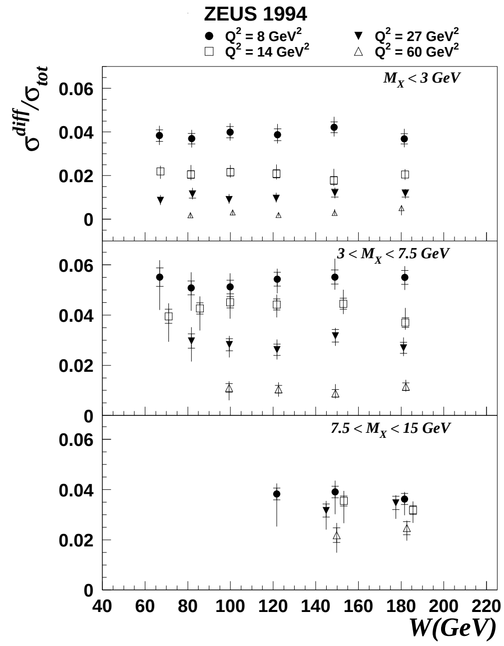

Fig. 19. The ratio of the diffractive cross section, integrated over the M_X intervals indicated, $\sigma^{\rm diff} = \int_{M_a}^{M_b} dM_X \sigma^{\rm diff}_{\gamma^* p\to XN}$, for $M_N < 5.5$ GeV, to the total cross section for virtual photon proton scattering, $r^{\rm diff}_{\rm tot} = \sigma^{\rm diff}/\sigma^{\rm tot}_{\gamma^* p}$, as a function of W for the M_X intervals and Q^2 values indicated. From ZEUS.

ing only on $x_{I\!P}$ and a structure function $F_2^{D(2)}$ which depends on (β, Q^2). The rise of $x_{I\!P} F_2^{D(3)}$ with $x_{I\!P}$ can be described as $x_{I\!P} F_2^{D(3)} \propto (1/x_{I\!P})^n$ with $n = 0.253 \pm 0.017({\rm stat})^{+0.077}_{-0.023}({\rm syst})$. The data are also consistent with models which break factorization.

Figure 21 shows $F_2^{D(2)}(\beta, Q^2) = x_0 F_2^{D(3)}(x_0, \beta, Q^2)$ where $F_2^{D(3)}$ was evaluated at $x_{I\!P} = x_0 = 0.0042$. The data show that $F_2^{D(2)}$ has a simple behaviour. For $\beta < 0.6$ and $Q^2 < 14$ GeV^2, $F_2^{D(2)}$ is approximately independent of β. For $\beta < 0.8$ also, the data from different Q^2 values are rather similar suggesting a leading twist behaviour characterized by a slow $\ln Q^2$ type rescaling. For $\beta > 0.9$, the data show a decrease with β or Q^2. The approximate constancy of $F_2^{D(2)}$ for $\beta < 0.9$ combined with the rapid rise of $F_2^{D(3)}$ as $x_{I\!P}$ decreases can be interpreted as evidence for a substantial partonic component in DIS diffraction dissociation.

The data were compared with several partonic models of diffraction, NZ [55], BPR [56] and BEKW [57]. Good agreement with the data can be

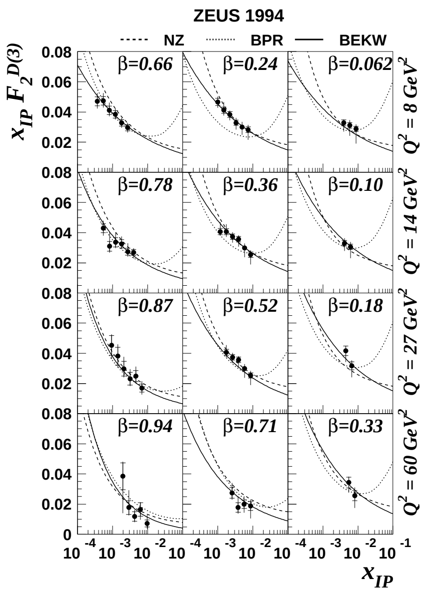

Fig. 20. The diffractive structure function of the proton multiplied by $x_{I\!P}$, $x_{I\!P} F_2^{D(3)}$, as a function of $x_{I\!P}$. The curves show the results from the models of Nikolaev and Zhakarov (NZ), Bialas, Peschanski and Royon (BPR) and Bartels, Ellis, Kowalski and Wüsthoff (BEKW).

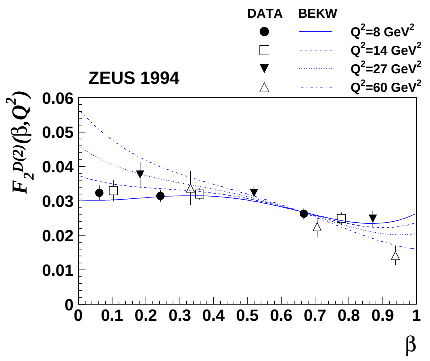

Fig. 21. The structure function $F_2^{D(2)}(\beta, Q^2)$ for $\gamma^* p \to XN, M_N < 5.5$ GeV, for the Q^2 values indicated, as a function of β as extracted from a fit to the measured $x_{I\!P} F_2^{D(3)}$ values. The curves show the fit results obtained with the BEKW model. From ZEUS.

achieved. The models provide a first glimpse of how the different components may build up the diffractive structure function.

The Q^2 behaviour of $x_{I\!P} F_2^{D(3)}(x_{I\!P}, \beta, Q^2)$ is different from that of the proton structure function $F_2(x, Q^2)$, taken at $x = x_{I\!P}$, which rises gradually

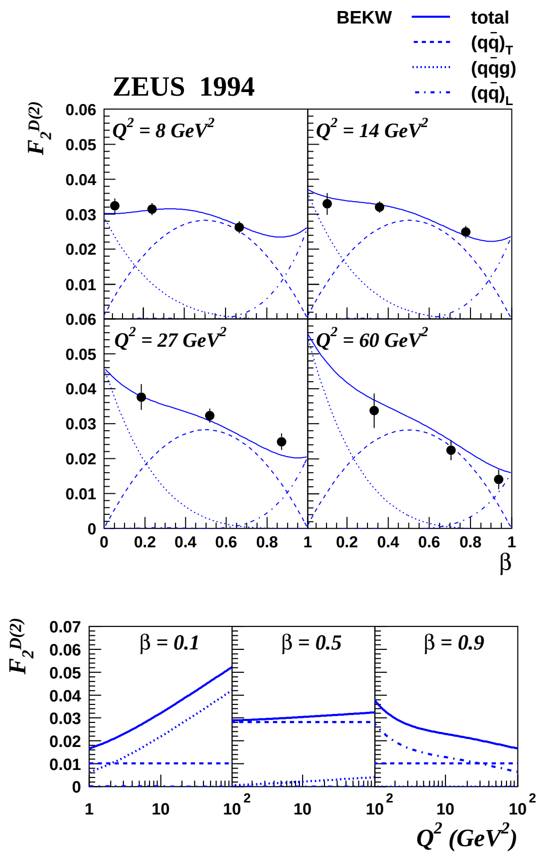

Fig. 22. Top: The three components $(q\overline{q})_T$, $(q\overline{q}g)$ and $(q\overline{q})_L$ of the BEKW model building up the diffractive structure function of the proton and their sum $F_2^{D(2)}(\beta, Q^2)$ as a function of β for $Q^2 = 8, 14, 27$ and 60 GeV^2, as obtained from a fit of the BEKW model to the data. Bottom: the same quantities as a function of Q^2 for $\beta = 0.1, 0.5$ and 0.9. From ZEUS.

with Q^2. It is in broad agreement with the conjecture [54] that

$$x_{I\!P} F_2^{D(3)}(x_{I\!P}, \beta, Q^2) \propto \frac{F_2(x = x_{I\!P}, Q^2)}{\log_{10}\left(\frac{Q^2}{Q_0^2}\right)}, \text{ where } Q_0^2 = 0.55 \text{ GeV}^2 .$$

In the BEKW model basically three components build up the diffractive structure function, $x_{I\!P} F_2^{D(3)}(\beta, x_{I\!P}, Q^2) = c_T \cdot F_{q\overline{q}}^T + c_L \cdot F_{q\overline{q}}^L + c_g \cdot F_{q\overline{q}g}^T$; the three terms represent the contributions from transverse photons fluctuating into a $q\overline{q}$ or a $q\overline{q}g$ system and from longitudinal photons fluctuating into a $q\overline{q}$ system. In the model, the three terms are given in terms of $x_{I\!P}, \beta$ and

Q^2 together with additional free parameters which were determined from a fit to the data.

It is instructive to compare the β and Q^2 dependences of the three components. Figure 22(top) shows $c_T F^T_{q\bar{q}}$ (dashed), $c_L F^L_{q\bar{q}}$ (dashed-dotted), $c_g F^T_{q\bar{q}g}$ (dotted) and their sum $x_{I\!P} F_2^{D(3)}(x_{I\!P}, \beta, Q^2)$ at $x_{I\!P} = x_0$ (solid curves) as a function of β for $Q^2 = 8, 14, 27, 60$ GeV^2. For $\beta > 0.2$ the colourless system couples predominantly to the quarks in the virtual photon. The region $\beta \geq 0.8$ is dominated by the contributions from longitudinal photons. The contribution from coupling of the colourless system to a $q\bar{q}g$ final state becomes important for $\beta < 0.3$. The last result is in contrast to the H1 observation (see above) that the large β region is dominated by the gluon contribution. Figure 22(bottom) shows the same quantities as a function of Q^2 for $\beta = 0.1, 0.5, 0.9$. The gluon term, which dominates at $\beta = 0.1$ rises with Q^2 while the quark term, which is important at $\beta = 0.5$ shows no evolution with Q^2, *i.e.* is of leading twist. The contribution from longitudinal photons, which is higher twist and dominates at $\beta = 0.9$, decreases with Q^2.

In the BEKW model the $x_{I\!P}$-dependence of the quark and gluon contributions for transverse photons is expected to be dominated by the aligned jet configuration [58] and, therefore, to be close to that given by the soft pomeron. Writing $F^T_{q\bar{q}} \propto (x_0/x_{I\!P})^n_T$ this implies $n_T \approx 2(\overline{\alpha_{I\!P}}^{\rm soft} - 1)$. However, perturbative admixtures in the diffractive final state are expected to have a somewhat stronger energy dependence, leading to an effective $n_T > 2(\overline{\alpha_{I\!P}}^{\rm soft} - 1)$. The $x_{I\!P}$ dependence of the longitudinal contribution is driven by the square of the proton's gluon momentum density leading to $n_L > n_T$. The fit of the BEKW model to the data indicates that transverse (longitudinal) photons dominate the region $\beta < 0.8$ ($\beta > 0.8$). Therefore different powers of n should be observed for the two regions. Assuming $n = n_T = n_L$ ZEUS found $n(\beta \geq 0.8) = 0.46 \pm 0.12$ and $n(\beta < 0.8) = 0.27 \pm 0.03$, a result which is consistent with the theoretical conjecture but lacks precision. It is important to note that already at $Q^2 = 8$ GeV^2, $n_T(Q^2 = 8\ \text{GeV}^2) = 0.25 \pm 0.04$ which is substantially larger than the expectation for soft contributions, $n_{soft} = 0.152^{+0.024}_{-0.018}$, indicating that the transverse and gluon components receive sizeable contributions from perturbative processes.

5. Deep inelastic scattering at high-Q^2, high-x

The results on structure functions of the proton presented in Section 3 have been obtained in NC scattering at Q^2 values below 5000 GeV^2 in a kinematical region which is dominated by photon-exchange. As one climbs up to Q^2 values of the order of M^2_W, M^2_Z, contributions from vector-boson exchange become important. During 1994-96, H1 and ZEUS have collected sufficient data for a first look at deep inelastic e^+p scattering beyond Q^2 values of 10 000 GeV^2. As Q^2 increases, finer and finer details in the proton (electron) can be resolved: for $Q^2 > 10000$ GeV^2 objects smaller than $2 \cdot 10^{-16}$, corresponding to a fraction of 10^{-3} of the proton diameter, can be resolved. In this regime, lepton-nucleon scattering allows unique and sensitive tests of the Standard Model (SM) as well as of certain extensions of it [59].

First results for the high Q^2 regime were presented by H1 and ZEUS in [60, 61] from data obtained in 1994-96 for integrated luminosities of 14 and 20 pb^{-1}, respectively. Both experiments reported good agreement with the SM predictions for $Q^2 < 15000$ GeV^2 and an excess of events in the region of $Q^2 > 15000$ GeV^2, $x > 0.4$.

With a luminosity of 14 pb^{-1} H1 observed 12 events with $Q^2 > 15000$ GeV^2 where only 4.7 ± 0.76 were expected from SM calculations. Assuming the SM to be correct, the probability for such an excess was found to be about 1%. Further, these high Q^2 events tended to cluster around x values of 0.4 - 0.5 corresponding to a positron-quark mass of $M \approx \sqrt{xs} \approx 200$ GeV which is suggestive for the production of a leptoquark or a R-parity violating SUSY state. In the region $187.5 < M < 212.5$ GeV, $y = Q^2/(xs) > 0.4$, 7 events were observed where 0.95 ± 0.18 were expected from SM processes.

The ZEUS experiment found for a luminosity of 20 pb^{-1} two events with $Q^2 > 35000$ GeV^2 while 0.145 ± 0.013 were expected from SM. For $x > 0.55$ and $y > 0.25$, four events were observed compared to 0.91 ± 0.08 expected. In the SM the probability for such a fluctuation to occur in this kinematic region was 0.7% and 8% for the entire region of $Q^2 > 5000$ GeV^2.

Thanks to the excellent performance of HERA, the data taken during the 1997 running period more than doubled the data samples. The preliminary results from these data combined with those from 1994-96 were presented by [1, 2]. They will be discussed in the following.

The combined data from 1994-97 from H1 [2, 63] corresponding to a luminosity of 37 pb^{-1} yielded a total of 322 events with $Q_e^2 > 5000$ GeV^2, $0.1 < y_e < 0.9$ [1] which is consistent with the 336 ± 29.6 events expected from SM. The distribution of y_e versus M_e is displayed in Fig. 23. For $Q_e^2 > 15000$ GeV^2 22 events were observed while 14.8 ± 2.1 were expected which corresponds to a probability of 6% that these events result from SM processes. Although the luminosity had more than doubled, the number of excess events did not increase when the 1997 data were added.

The situation is similar with the data from ZEUS which correspond to an integrated luminosity of 47 pb^{-1} after adding the data from 1997. Figure 24

[1] The index "e" indicates the determination of the kinematic variable by the electron method.

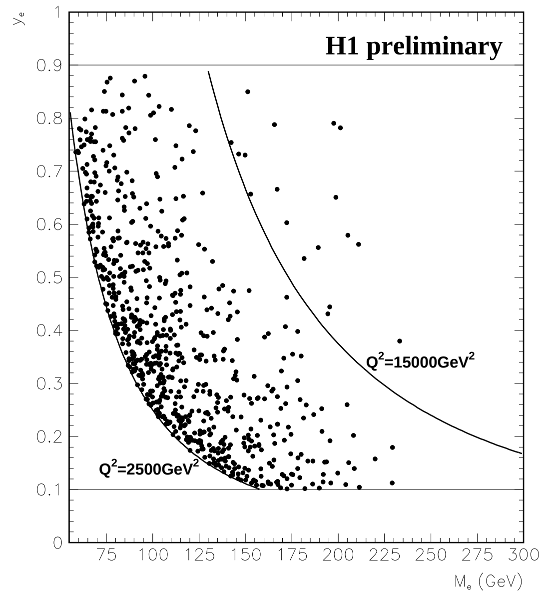

Fig. 23. Process $e^+p \to eX$, preliminary results from H1: distribution of y_e versus M_e.

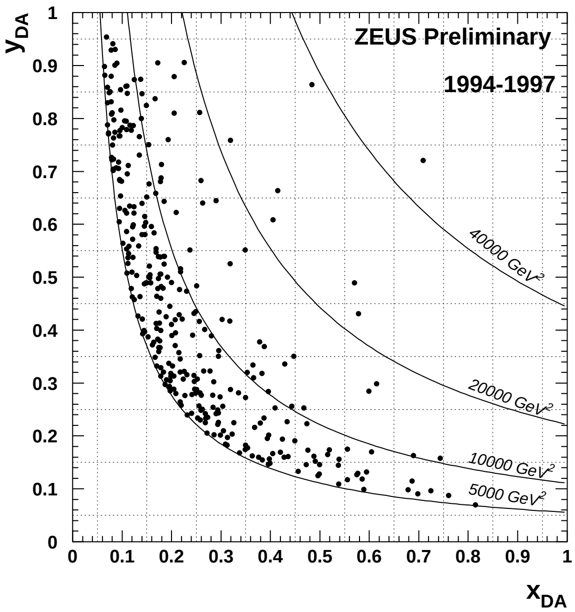

Fig. 24. Process $e^+p \to eX$: distribution of x_{DA} versus y_{DA} for the 1994-97 data. Preliminary results from ZEUS.

shows the distribution of the events in the x_{DA}, y_{DA} [2] plane [62]. There are 440 events with $Q^2 > 5000$ GeV^2 to be compared with 396 ± 24 expected. For $Q^2 > 15000$ the numbers are 20 events observed and 17 ± 2 expected; for $Q^2 > 35000$ GeV^2 2 events are observed and 0.29 ± 0.02 are expected. Hence, no new outstanding events were observed in the 1997 data.

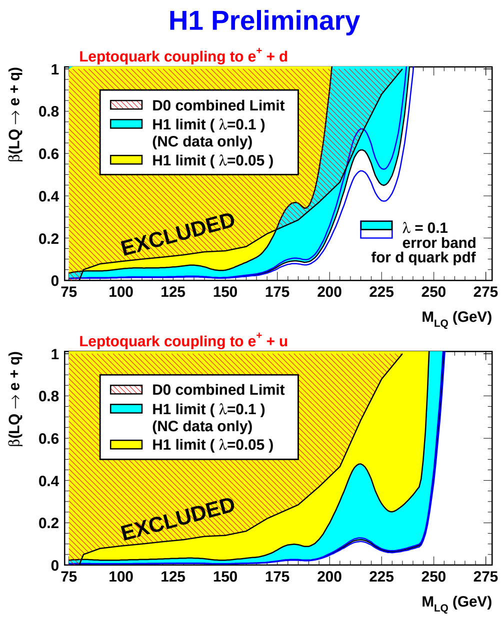

Fig. 25. Rejection limits for the branching ratio β vs mass M_{LQ} for a first generation scalar leptoquark. From H1.

H1 used their data to place an upper limit on the branching ratio β for a possible leptoquark coupling to e^+d or e^+u. The cross section for production of a scalar leptoquark by e^+p scattering can be written as [64]; for a scalar LQ:

$$\frac{d\sigma(ep \to LQ)}{dxdy} = \frac{1}{32\pi} q(x,y) \frac{\lambda^4 \, xs}{(xs - M_{LQ}^2)^2 + M_{LQ}^2 \Gamma_{LQ}^2}\,, \tag{11}$$

where $q(x,y)$ is the density of quark q in the proton, $M_{LQ} = xs$ and Γ_{LQ} are the LQ mass and width, and λ measures the eq coupling strength for a particular combination of the e and q helicities. Figure 25 shows limits on β as a function of the mass M_{LQ} for λ values of 0.1 and 0.05. Also shown are recent limits from the TEVATRON [65, 66]. For small values of β the H1 limits are more stringent.

[2] The index "DA" indicates the determination of the kinematic variables with the double-angle method.

In conclusion, integrated luminosities of 50 - 100 pb^{-1} are now required in order to either confirm the earlier excess of events at high-x, high-y or to lay the matter to rest.

I want to thank J. Blümlein and T. Riemann for a very enjoyable stay at Rheinsberg. Discussions with T. Doyle, H. Kowalski, B. Surrow, Y. Tsipolitis and W. Zeuner on the HERA data presented at the DIS98 Workshop in Brussels have been very helpful in preparing this talk.

REFERENCES

[1] A.T. Doyle, Highlights and Open Questions from ZEUS, Proc. DIS98 Workshop, Brussels 1998.

[2] T. Greenshaw, Results from H1, Proc. DIS98 Workshop, Brussels 1998.

[3] L. Demortier, A. Mehta, W. Zeuner, Structure Functions Summary - Part 1, Proc. DIS98 Workshop, Brussels 1998.

[4] G. Wolf, *Acta Phys. Pol.* **B28**, 2587 (1997).

[5] Ch. Berger, W. Wagner, *Phys. Rep.* **146**, 1 (1987); For a recent summary see S. Söldner-Rembold, hep-ex/9711005, invited talk given at the XVIII Intern. Symp. Lepton Photon Interactions, Hamburg, Germany, 1997.

[6] J. Breitweg *et al.*, ZEUS Collaboration, DESY 98-085.

[7] S. Frixione *et al.*, *Phys. Lett.* **B348**, 633 (1995) and *Nucl. Phys.* **B454**, 3(1995).

[8] H. Lai *et al.*, *Phys. Rev.* **D55**, 1280 (1997).

[9] M. Glück, E. Reya, A. Vogt, *Phys. Rev.* **D46**, 1973 (1992).

[10] S. Peterson *et al.*, *Phys. Rev.* **D27**, 105 (1983).

[11] B.A. Kniehl *et al.*, *Z. Phys.* **C76**, 689 (1997); J. Binnewies *et al.*, DESY 97-241, hep-ph/9712482, *Phys. Rev.* **D** (1998), in print.

[12] J. Binnewies *et al.*, *Z. Phys.* **C76**, 677 (1997).

[13] M. Cacciari *et al.*, *Phys. Rev.* **D55**, 2736 (1997); *Phys. Rev.* **D55**, 7134 (1997).

[14] G. Tsipolitis, Proc. DIS98 Workshop, Brussels, 1998.

[15] AROMA: G. Ingelman, J. Rathsman, G.A. Schuler, *Comput. Phys. Commun.* **101**, 135 (1997).

[16] HERWIG 5.9: G. Marchesini *et al.*, *Comput. Phys. Commun.* **67**, 465 (1992).

[17] ZEUS Collaboration, J. Breitweg *et al.*, *Z. Phys.* **C75**, 215 (1997).

[18] M.G. Ryskin, R.G. Roberts, A.D. Martin, E.M. Levin, RAL-TR-95-065.

[19] L.P.A. Haakman, A. Kaidalov, J.H. Koch, *Phys. Lett.* **B365**, 411 (1996).

[20] L.L. Jenkovszky, E.S. Martynov, F. Paccanoni, *Novy. Svet Hadrons* (1996) 170.

[21] ZEUS Collaboration, J. Breitweg *et al.*, DESY 98-089.

[22] L. Frankfurt, W. Koepf, M. Strikman, *Phys. Rev.* **D57**, 27 (1998); R. Engel, M. McDermott, private communication.

[23] F. Lehner, talk given at the Lake Louise Winter Institute, 1998, Canada.

[24] H1 Collaboration, C. Adloff *et al.*, *Z. Phys.* **C72**, 593 (1996).

[25] M. Glück, E. Reya, A. Vogt, *Z. Phys.* **C67**, 433 (1995).

[26] ZEUS Collaboration, J. Breitweg *et al.*, *Phys. Lett.* **B407**, 402 (1997).

[27] A. Vogt, Structure Functions Summary - Part II, Proc. DIS98 Workshop, Brussels, 1998.

[28] H1 Collaboration, C. Adloff *et al.*, *Nucl. Phys.* **B497**, 3 (1997).

[29] ZEUS Collaboration, J. Breitweg *et al.*, *Phys. Lett.* **B407**, 432 (1997).

[30] B. Surrow, PhD thesis, University of Hamburg, DESY-THESI-1998-004 (1998); B. Surrow, Investigations on the transisition from non-perturbative to perturbative QCD in inelastic e^+p-scattering at HERA, Proc. DIS98 Workshop, Brussels 1998.

[31] A. Donnachie, P.V. Landshoff, *Phys. Lett.* **B296**, 227 (1992).

[32] A. Caldwell, Invited talk at the DESY Theory Workshop on Recent Developments in QCD, October 1997 (unpublished).

[33] NMC Collaboration, M. Arneodo *et al.*, *Nucl. Phys.* **B483**, 3 (1997)..

[34] BCDMS Collaboration, A.C. Benvenuti *et al.*, *Phys. Lett.* **B223**, 485 (1989) and *Phys. Lett.* **B237**, 592 (1990).

[35] A.D. Martin *et al.*, DTP/98/10, RAL-TR-98-029 and hep-ph/9803445 (1998).

[36] G. Alberi, G. Goggi, *Phys. Rep.* **74**, 1 (1981); K. Goulianos, *Phys. Rep.* **101**, 169 (1983); *Nucl. Phys. B*, *Proc. Suppl.* **12**, 110 (1990); G. Giacomelli, University and INFN Bologna report DFUB 9-94 (1994).

[37] N. Gribov, *Sov. Phys. JETP* **14**, 478 (1962); *Sov. Phys. JETP* **14**, 1395 (1962); G.F. Chew, S. Frautschi, *Phys. Rev. Lett.* **7**, 394 (1961); R.D. Field, G. Fox, *Nucl. Phys.* **B80**, 367 (1974); A.B. Kaidalov, K.A. Ter-Martirosyan, *Nucl. Phys.* **B75** 471 (1974).

[38] A. Donnachie, P.V. Landshoff, *Nucl. Phys.* **B244**, 322 (1984); *Phys. Lett.* **B296**, 227 (1992).

[39] G. Ingelman, P. Schlein, *Phys. Lett.* **B152**, 256 (1985).

[40] UA8 Collaboration, R. Bonino *et al.*, *Phys. Lett.* **B211**, 239 (1988); A. Brandt *et al.*, *Phys. Lett.* **B297**, 417 (1992).

[41] ZEUS Collaboration, M. Derrick *et al.*, *Z. Phys.* **C69**, 39 (1995) 39; *Phys. Lett.* **B377**, 259 (1996); *Z. Phys.* **C73**, 73, 253 (1996); J. Breitweg *et al.*, *Eur. Phys. J.* **C2**, 247 (1998); H1 Collaboration, S. Aid *et al.*, *Nucl. Phys.* **B463**, 3 (1996).

[42] ZEUS Collaboration, M. Derrick *et al.*, *Phys. Lett.* **B356**, 601 (1995); *Phys. Lett.* **B380**, 220 (1996); H1 Collaboration, S. Aid *et al.*, *Nucl. Phys.* **B468**, 3 (1996); *Z. Phys.* **C75**, 607 (1997).

[43] ZEUS Collaboration, M. Derrick *et al.*, *Phys. Lett.* **B315**, 481 (1993).

[44] H1 Collaboration, T. Ahmed *et al.*, *Nucl. Phys.* **B429**, 477 (1994).

[45] ZEUS Collaboration, M. Derrick *et al.*, *Z. Phys.* **C68**, 569 (1995); *Z. Phys.* **C70**, 391 (1996).

[46] ZEUS Collaboration, M. Derrick *et al.*, *Phys. Lett.* **B332**, 228 (1994); *Phys. Lett.* **B338**, 483 (1994); J. Breitweg *et al.*, *Phys. Lett.* **B421**, 36 (1998).

[47] H1 Collaboration, T. Ahmed *et al.*, *Phys. Lett.* **B348**, 681 (1995).

[48] ZEUS Collaboration, *Z. Phys.* **C70**, 391 (1996).

[49] H1 Collaboration, C. Adloff *et al.*, *Z. Phys.* **C76**, 613 (1997).

[50] ZEUS Collaboration, J. Breitweg *et al.*, *Eur. Phys. J.* **C1**, 81 (1998).

[51] ZEUS Collaboration, J. Breitweg *et al.*, DESY 98-084.

[52] G. Ingelman, K. Janson-Prytz, Proc. Workshop "Physics at HERA", ed. W. Buchmüller, G. Ingelman, DESY 1992, Vol.1, p. 233; G. Ingelman, K. Prytz, *Z. Phys.* **C58**, 285 (1993).

[53] J. Cudell, K. Kang, S.K. Kim, Brown-HET-1060 and hep-ph/9701312.

[54] W. Buchmüller, *Phys. Lett.* **B353**, 335 (1995); W. Buchmüller, A. Hebecker, *Nucl. Phys.* **B476**, 203 (1996).

[55] N.N. Nikolaev, B.G. Zakharov, *Z. Phys.* **C53**, 331 (1992); M. Genovese, N.N. Nikolaev, B.G. Zakharov, JETP81 (1995) 625.

[56] A. Bialas, R. Peschanski, *Phys. Lett.* **B387**, 405 (1996); A. Bialas, R. Peschanski, Ch. Royon, *Phys. Rev.* **D57**, 6899 (1998).

[57] J. Bartels, J. Ellis, H. Kowalski, M. Wüsthoff, CERN-TH/98-67, DESY 98-034, DTP 98-02 and hep-ph/9803497.

[58] J.D. Bjorken, Proc. Int. Symp. Electron and Photon Interactions at High Energies, Cornell, 1971, p. 282; J.D. Bjorken, J. Kogut, D. Soper, *Phys. Rev.* **D3**, 1382 (1971). J.D. Bjorken, J. Kogut, *Phys. Rev.* **D8**, 1341 (1973).

[59] Future Physics at HERA, ed. G. Ingelman, A. DeRoeck, R. Klanner, (DESY Hamburg, 1996), and references therein; R. Cashmore *et al.*, *Phys. Rep.* **122**, 275 (1985).

[60] H1 Collaboration, C. Adloff *et al.*, *Z. Phys.* **C74**, 191(1997).

[61] ZEUS Collaboration, J. Breitweg *et al.*, *Z. Phys.* **C74**, 207 (1997).

[62] A. van Sighem, Lake Louise Winter Institute, 1998, Alberta, Canada.

[63] P. Bruel, Rencontres de Moriond, Les Arc, 1998.

[64] W. Buchmüller, R. Rückl, D. Wyler, *Phys. Lett.* **B191**, 442 (1987).

[65] CDF Collaboration, F. Abe *et al.*, *Phys. Rev. Lett.* **79**, 4327 (1997).

[66] D0 Collaboration, B. Abbott *et al.*, *Phys. Rev. Lett.* **80**, 2051 (1998).